Dynamic patterns in a supported lipid bilayer driven by standing surface acoustic waves†

Martin Hennig,‡[b] Jürgen Neumann,‡[a] Achim Wixforth,[a] Joachim O. Rädler[b] and Matthias F. Schneider*[a]

DOI: 10.1039/b907157a

In the past decades supported lipid bilayers (SLBs) have been an important tool in order to study the physical properties of biological membranes and cells. So far, controlled manipulation of SLBs is very limited. Here we present a new technology to create lateral patterns in lipid membranes controllable in both space and time. Surface acoustic waves (SAWs) are used to generate lateral standing waves on a piezoelectric substrate which create local "traps" in the lipid bilayer and lead to a lateral modulation in lipid concentration. We demonstrate that pattern formation is reversible and does not affect the integrity of the lipid bilayer as shown by extracting the diffusion constant of fluid membranes. The described method could possibly be used to design switchable interfaces for the lateral transport and organization of membrane bound macromolecules to create dynamic bioarrays and control biofilm formation.

The generation of switchable interfaces enables the active control of biofilm formation and macromolecule adsorption to solid supported lipid membranes. Furthermore, it allows the design of new model systems to study the heterogeneity of biological membranes and their dynamics, which play an extraordinary role for many biochemical and biological processes.[1] Lateral organization of the cell membrane, including lipid rafts, represent essential biological functions[2–5] and are able to modulate enzyme catalysis or receptor mobility, which has been shown to be one of the key players in cell adhesion.[6] Understanding these processes would not only be of great general interest, but also allow many life science applications. Initial membrane structuring efforts have been done by [7–9], but to date, there has been no successful dynamical approach.

Supported lipid membranes (SLBs) have been intensively studied over the last decades with the aim of mimicking the physical properties of lipid membranes.[10–14] Lateral microstructuring of SLBs with and without attached macromolecules was demonstrated to be feasible by nanostructuring of the solid support.[7,15,32] However, these patterns are temporally and spatially fixed. Electrophoretic migration enables the manipulation of the membrane in-plane actively, although it gives no flexibility as far as pattern symmetry (lattice constants) and domain dimensions (line vs dot) are concerned.[9,16,17] There are, however, currently no available tools for actively controlling the spatial and temporal organisation in supported membranes. Dynamical control over SLBs would allow local enrichment of membrane proteins, *e.g.* ion channels or receptors. Chip-based transport of membrane components could be envisioned as integrated tool for membrane-protein purification or size separation of proteins.

One of the most promising tools for micro and nanoscale manipulation, as well as surface sensing, are surface acoustic waves (SAWs). SAW based sensors, for instance, exploit the interaction between "soft" adsorbed coats and the solid substrate to extract viscous (attenuation factor) and elastic (sound velocity) properties of the adsorbed film very similar to quartz crystal microbalances.[18] In a fluidic environment, usually shear surface acoustic waves (sSAWs) are employed as they provide minimal viscous damping. Significant progress has been made since the beginning of SAW sensing, demonstrating that SAW shear wave chips are potential candidates for biotechnological applications as well.[19] SAW technology is particularly useful for lab on a chip applications, as it is cheap and minimizes mechanical parts such as pumps or pipes. SAWs can be directly used as nanopumps to drive microfluidic devices and mix liquids.[20–22] Furthermore, it has recently been demonstrated that Rayleigh SAWs are able to align latex beads or carbon nanotubes in microfluidic channels, [23–25] the driving force being pressure waves in these cases.

In this article, we apply shear surface acoustic waves (sSAWs) to reversibly induce well-defined lateral density gradients in supported lipid bilayers. To this end, we designed standing sSAW chips that allow for optical observation with high numerical aperture, enabling imaging of the emergence and decay of patterns in the fluorescent lipid tracer intensity. Using high resolution fluorescence microscopy membrane dynamics was analyzed as well.

One of the best substrates for sSAW applications is $LiTaO_3$ (lithium tantalate) due to its high k^2 and ε. At both ends of our chip, interdigital transducers (IDTs) excite sSAWs, which counter propagate and form a standing wave (Fig. 1a) that can be visualized by AFM in air (Fig. 1c), as well as under water

[a]*Center for Nanoscience, CeNS, Universität Augsburg, Institut für Physik, Universitätsstr. 1, D-86159 Augsburg, Germany. E-mail: Matthias.Schneider@physik.uni-augsburg.de*

[b]*Center for Nanoscience, CeNS, Ludwig-Maximilians-Universität, Fakultät für Physik, Geschwister Scholl Platz 1, D-80539 München, Germany*

† Electronic supplementary information (ESI) available: Movie showing the formation and decay of lateral patterns in a lipid membrane subjected to a standing surface acoustic shear wave (sSAW). See DOI: 10.1039/b907157a

‡ These authors contributed equally to this work.

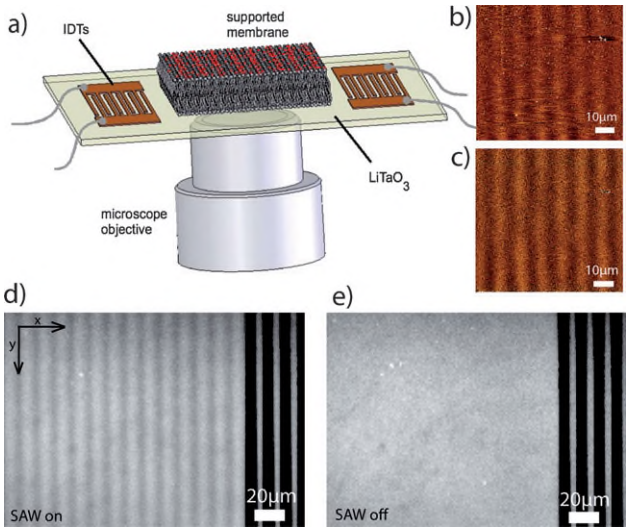

Fig. 1 a) Diagram showing the experimental setup, including the piezoelectric chip and the inverted microscope. The interdigital transducers excite a standing SAW, which induces lateral demixing of the supported lipid membrane. b) Shear waves visualized by AFM under water in lateral deflection mode. The pattern periodicity is half of the wavelength of the SAW (13.3 µm). c) AFM-image of shear SAWs in air. d) Typical micrograph of a fluorescently-labelled demixed membrane after the SAW has been switched on. The membrane pattern correlates with the periodicity of the IDTs (black stripes on the right side). e) When the SAW is switched off, the dye relaxes within seconds into its equilibrium distribution.

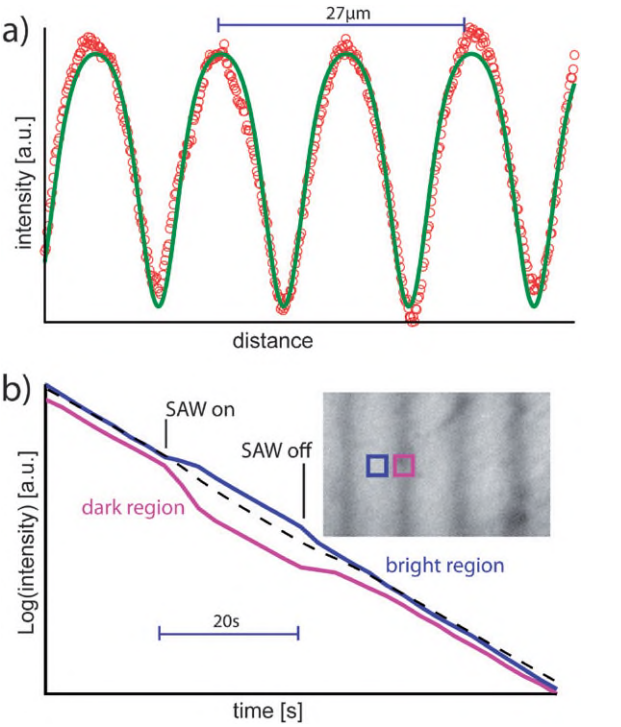

Fig. 2 a) Typical intensity profile of a SAW-demixed membrane (data points). The intensity profile can be fitted to $I(x) \propto \exp(\sin^2 x)$ (line, for details refer to the text). b) Temporal evolution of the integrated fluorescence intensity of a node and antinode (inset). The dotted line shows the average for the node and antinode, demonstrating that lipids are redistributed. The overall intensity decrease results from bleaching.

(Fig. 1b). As a consequence of the weak coupling to the bulk phase, the standing sSAW extends over many periods. When supported membranes containing 0.5% of labelled lipids created by the vesicle fusion method [12–17] (Fig. 1a/d) were exposed to the generated standing sSAWs, vertical stripes of increased and decreased fluorescence intensity arise after less than 1 s, indicating an acoustically driven lateral reorganisation of the lipid bilayer (Fig. 1d).

The fluorescence intensity profile exhibits twice the periodicity of the standing wave (Fig. 1d, 2a) and we observe a significant asymmetry between darker and brighter regions. This resulting intensity profile, $I_f(x)$ can be well approximated by

$$I_F(x) = I_0 - I_1 \exp(-k^2 \beta \sin^2 kx) \qquad (1)$$

as shown in Fig. 2a and consistent with a SAW induced demixing, as described in the following: according to Nissen *et al.*[27] Texas Red labelled DHPE exponentially accumulates in regions of low membrane density. These regions are located in the nodes of the standing wave pattern (Fig. 1d), whereas the $\sin^2 kx$ perfectly reflects the double standing sSAW periodicity. Comparing the fluorescence intensities as a function of time at two different spots (Fig. 2b) demonstrates that the SAW driven dye separation can be clearly distinguished from possible regular bleaching effects. Furthermore, no pronounced intensity changes are observed at the time when the SAW is switched on or off indicating that the strain field does not modulate the emission of the fluorescence dye itself. Hence, we conclude that the lipid dye is redistributed by the local in-plane forces induced by the SAW. The fact, that the fluorescence intensity visibly decreases and redistributes with typical membrane diffusion constants, shows that the bilayer remains intact over time. Only a real in-plane dye redistribution gives a plausible explanation, as *e.g.* changes in thickness of the membrane wouldn't affect the dye's fluorescence intensity signal. A rupture of the bilayer and reorganisation into multilayers would be clearly visible in the micrograph as regions of double or multiple intensity in contradiction to the observed smooth redistribution.

Qualitatively, equation 1 can be explained by assuming that the local strain field in the substrate couples through the approx. 0.5–2 nm thin water layer[34] into the lipid bilayer. In the linear regime, the time averaged energy $\langle F \rangle$ of a lateral strain field caused by standing SAWs along the x-axis is

$$\langle F \rangle_t \propto k^2 \sin^2 kx \qquad (2)$$

Therefore, the highest energy dissipation on the SLB occurs at the nodes of the standing sSAW, where the strain is maximal. Whether the energy transport is dissipative, inducing a lateral temperature modulation, or elastic, creating a modulation in lateral density, leads to the same qualitative result, and requires a microscopic description of the coupling mechanism.[28,29] Thermodynamically, a lateral modulation in stress energy in the lipid membrane requires a redistribution of the dye according to Boltzmann and consequently, an intensity variation of the form found experimentally (Eq. 1). In Fig. 3a, we show the temporal evolution of pattern formation and decay. Each vertical line

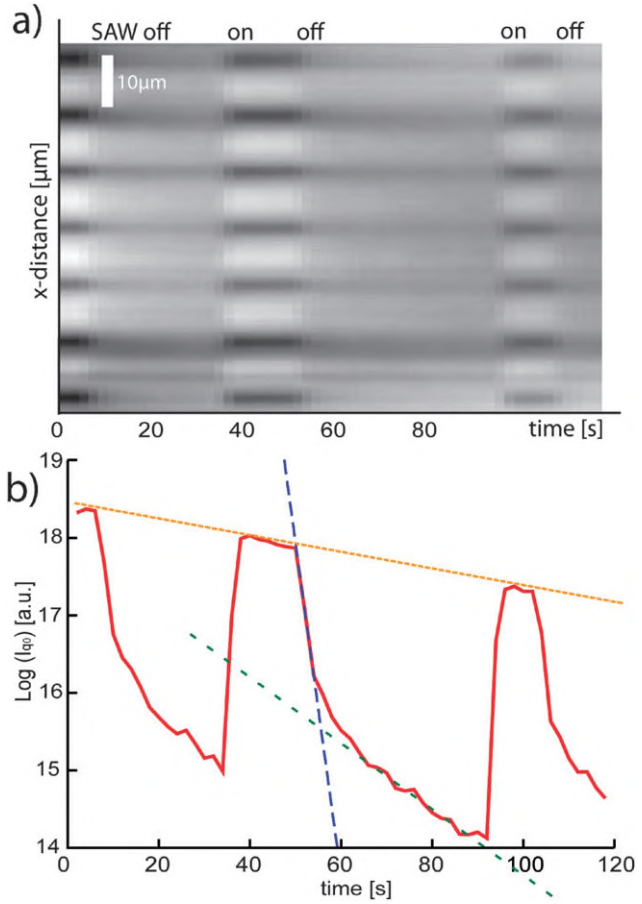

Fig. 3 a) Time series of switch on-and-off processes. Each vertical line represents the averaged intensity along the vertical axis (Fig. 1d). The framerate is 2 s. b) Time evolution of the fundamental Fourier component of the intensity pattern in Fig. 3a. The dotted line indicates bleaching (yellow). It shows the same slope as in Fig. 2b. The Fourier component decay indicates two distinct diffusive processes with $D_1 \approx 2\ \mu m^2/s$ and $D_2 \approx 0.2\ \mu m^2/s$ (dashed lines, blue and green).

represents the integration $\int_0^L I(y)dy$ of a snapshot as depicted in Fig. 1d and e. Here, L is the total extension of the image in y-direction. In the figure, the measured intensities are plotted as a function of time and the intervals of SAW application are indicated. Fig. 3b depicts the amplitude of the fundamental spatial frequency k_0 as a function of time. The decrease of k_0 after the SAW power has been switched off exhibits two time scales, which follow an exponential decay. This finding is indicated by straight lines in the semi-logarithmic representation. Such an exponential decay is expected for a diffusive process, in which case the intensities of the Fourier components follow

$$c_k(t) = c_k^0 \exp(-k^2 D t) \tag{3}$$

From the first decay rate, we obtain $D_1 = 2\ \mu m/s^2$, which is consistent with literature values for typical diffusion constants (1–5 $\mu m/s^2$ [30,33]) of supported membranes measured by FRAP, FCS or continuous bleaching. The second observed timescale corresponds to a diffusive process with $D_2 = 0.2\ \mu m/s^2$, which could possibly be attributed to diffusion in the monolayer leaflet adjacent to the substrate. The existence of two distinct mobilities in a supported bilayer has been reported before[30] and becomes plausible concerning the fact that the viscosity of bulk water and surface-bound nanoscopic water layers differs by at least one order of magnitude.[35] At least in this case of high membrane viscosity the diffusion constant scales as $1/\eta$ where η is the viscosity of the adjacent medium.[34] Therefore a decrease in diffusion constant of the same order as the viscosity increases is expected in reasonable accordance with our experimental observations. An alternative explanation could be SAW induced nanoscopic membrane defects that heal after the SAW has been switched off. For our samples, we use 15 × 15 mm $LiTaO_3$ 36° Y-cut, X-propagation crystal (Roditi, London) sSAW-chips on which predominantly shear waves are generated.[31,29] The substrates are 200–400 µm thick, transparent and mirror-polished on both sides. For the standing wave generation, a typical delay line setup was fabricated by using a standard lithography and lift-off process. Lithography masks were produced by ebeam lithography. For the IDTs and electrical connections, we use a stack of 10 nm titanium adhesion layer, 50 nm gold and another 10 nm titanium capping layer. After the lift-off process and an oxygen plasma-cleaning step, rf-sputtering was used to deposit approximately 150 nm SiO_2 on top of the IDTs and the delay line region. Each IDT consists of 30 finger pairs with a periodicity of 26.6 µm, having an aperture of 978 µm and an insertion loss of about 30 dB at an operating frequency of 153 MHz. The active region between the IDTs is 3.5 mm long. The device is mounted on an epoxy printed circuit board with dimensions of a standard microscopy slide. The liquid reservoir consists of an open, biocompatible polydimethylsiloxane (PDMS) cylinder, which adheres tightly to the substrate. Standing waves were generated by continuous and simultaneous rf stimulation on both IDTs (Rohde&Schwarz, SML02). The generator output was amplified (Mini-Circuits, ZHL-2) and split (Mini-Circuits, ZFSC-2-4) to provide frequency and phase stability. The phase and coupling conditions in dry state are very distinct from the conditions under water, but the pattern location was determined using AFM in deflection mode to be temporally and locally stable in both cases (Fig. 1b).

Supported lipid bilayers were prepared by the vesicle fusion method as reported in ref. 12–17,26,32. Lipids (Avanti Polar Lipids, Alabaster, AL) were mixed in chloroform, dried under vacuum and tip-sonicated in water to create small unilamellar vesicles. A mixture of soy bean extract, CTAB (cetyltrimethylammonium bromide, Roth) and Texas Red-labelled DHPE (1,2-dihexadecanoyl-sn-glycero-3-phosphoethanolamine, triethylammonium salt, 90/9/1 mol%, Invitrogen) was found to form the most reliable supported bilayers at a final concentration of 1 mg/ml in water. The SAW chambers were filled with the solution for 45 min, then rinsed with water. The resulting bilayer was allowed to stabilize a few hours, usually overnight. Nearly identical results could be obtained using a DOPC/TR (1,2-dioleoyl-sn-glycero-3-phosphocholine) or a SOPC/TR (1-stearoyl-2-oleoyl-sn-glycero-3-phosphocholine) mixture, indicating that neither the heterogeneous mixture of the soy bean extract nor the cationic lipids cause the demixing. An inverted Zeiss Axiovert 100M microscope (Zeiss, Oberkochen) and a cooled 12 bit CCD camera (Sensicam qe, PCO, Kelheim) was used for high-resolution fluorescence microscopy.

Conclusions

In summary, we applied standing sSAWs to supported lipid bilayers and observed lateral membrane demixing, the controlled pattern formation and decay using high resolution fluorescence microscopy. The latter reveals diffusion times of supported bilayers, which are consistent with those obtained from FCS or FRAP, and therefore demonstrates a novel method for measuring diffusion constants of SLBs.

Furthermore, by shifting the phases and/or the frequency of the two counter propagating SAWs will allow to switch between standing wave patterns of different distance which can be moved with respect to the substrate. We picture a new model to mimic the dynamics of the cell membrane: macromolecules attached to functionalized lipids can be reversibly transported and assembled in two dimensions to create lateral organization with active clusters of binding sites or receptors embedded in an intact fluid lipid bilayer. In terms of applications, we envision to use this technology to design novel particle filters or to control biofilm formation. Finally, as an outlook, increasing the excitation frequency to about 3 GHz, the lateral resolution can be down-scaled to less than 100 nm allowing organization beyond optical resolution.

Acknowledgements

Financial support by the Cluster of Excellence "Nanosystems Initiative Munich, NIM" and the German Science Foundation DFG is gratefully acknowledged. JN thanks the IDK-NBT for funding. MFS personally likes to thank the Bavarian Research Foundation. We thank S. Manus for technical support.

References

1 T. D. Pollard, W. C. Earnshaw, J. Lippincott-Schwartz, *Cell Biology*, Saunders, Elsevier, USA, 2008.
2 K. Jacobson, O. G. Mouritsen and R. G. W. Anderson, *Nature Cell Biology*, 2007, **9**(1), 7–14.
3 K. Simons and D. Toomre, *Nat Rev Mol Cell Biol*, 2000, **1**(1), 31–39.
4 K. Simons and E. Ikonen, *Nature*, 1997 Jun 5, **387**(6633), 569–572.
5 K. Jacobson and C. Dietrich, *Trends Cell Biol*, 1999, **9**(3), 87–91.
6 A. Smith, K. Sengupta, S. Goennenwein, U. Seifert and E. Sackmann, *Proc Natl Acad Sci USA*, 2008, **105**(19), 6906–6911.
7 J. T. Groves, N. Ulman and S. G. Boxer, *Science*, 1997, **275**(5300), 651–653.
8 M. L. Kraft, P. K. Weber, M. L. Longo, I. D. Hutcheon and S. G. Boxer, *Science*, 2006, **313**(5795), 1948–1951.
9 J. T. Groves and S. G. Boxer, *Biophys J*, 1995, **69**(5), 1972–1975.
10 A. A. Brian and H. M. McConnell, *Proc Natl Acad Sci U S A*, 1984, **81**(19), 6159–6163.
11 H. M. McConnell, T. H. Watts, R. M. Weis and A. A. Brian, *Biochim Biophys Acta*, 1986, **864**(1), 95–106.
12 E. Sackmann, *Science*, 1996, **271**(5245), 43–48.
13 J. O. Raedler, H. Strey and E. Sackmann, *Langmuir*, 1995, **11**(11), 4539–4548.
14 C. Reich, M. R. Horton, B. Krause, A. P. Gast, J. O. Raedler and B. Nickel, *Biophys J*, 2008, **95**(2), 657–668.
15 M. B. Hochrein, J. A. Leierseder, L. Golubovic and J. O. Raedler, *Phys Rev Lett*, 2006, **96**(3), 038103.
16 J. T. Groves, S. G. Boxer and H. M. McConnell, *Proc Natl Acad Sci USA*, 1998, **95**(3), 935–938.
17 S. G. Boxer, *Curr Opin Chem Biol*, 2000, **4**(6), 704–709.
18 A. Janshoff, H. Galla and C. Steinem, *Angewandte Chemie*, 2000, **39**(22), 4004–4032.
19 E. Gizeli, F. Bender, A. Rasmusson, K. Saha, F. Josse and R. Cernosek, *Biosens Bioelectron*, 2003, **18**(11), 1399–1406.
20 A. Wixforth, C. Strobl, C. Gauer, A. Toegl, J. Scriba and Z. von Guttenberg, *Analytical and Bioanalytical Chemistry*, 2004, **379**(7–8), 982–991.
21 Z. von Guttenberg, H. Müller, H. Habermüller, A. Geisbauer, J. Pipper, J. Felbel, M. Kielpinski, J. Scriba and A. Wixforth, *Lab Chip*, 2005, **5**(3), 308–317.
22 T. Frommelt, M. Kostur, M. Wenzel-Schafer, P. Talkner, P. Haenggi and A. Wixforth, *Physical Review Letters*, 2008, **100**(3), 034502.
23 C. J. Strobl, C. Schaeflein, U. Beierlein, J. Ebbecke and A. Wixforth, *Applied Physics Letters*, 2004, **85**(8), 1427–1429.
24 J. Shi, X. Mao, D. Ahmed, A. Colletti and T. J. Huang, *Lab Chip*, 2008, **8**(2), 221–223.
25 C. D. Wood, S. D. Evans, J. E. Cunnigham, R. O'Rorke, C. Walti and A. G. Davies, *Applied Physics Letters*, 2008, **92**(4), 44104 1–3.
26 B. Maier and J. O. Raedler, *Phys. Rev. Lett.*, 1999, **82**(9), 1911–1914.
27 J. Nissen, S. Gritsch, G. Wiegand and J. O. Raedler, *European Physical Journal B*, 1999, **10**, 335–344.
28 O. Kolosov and K. Yamanaka, *Japanese Journal of Applied Physics Part 2-Letters*, 1993, **32**(8A), L1095–L1098.
29 S. Shiokawa and T. Moriizumi, *Japanese Journal of Applied Physics (Supplemental; Proc. 8th Symp. Ultrason. Electron.)*, 1988, **27**(1), 142–144.
30 M. Stelzle, R. Miehlich and E. Sackmann, *Biophys. J.*, 1992, **63**, 1346–1354.
31 T. Nomura, T. Yasuda, 1990, *Ultrasonics Symposium*, IEEE307–310.
32 B. Sanii, A. M. Smith, R. Butti, A. M. Brozell and A. N. Parikh, *Nano Lett.*, 2008, **8**(3), 866–871.
33 R. Merkel, E. Sackmann and E. Evans, *Journal de Physique*, 1989, **50**, 1535–1555.
34 B. D. Hughes, B. A. Pailthorpe and L. R. White, *Journal Of Fluid Mechanics*, 1981, **110**, 349–372.
35 J. S. Clegg and W. Drost-Hansen, *Biochemistry and Molecular Biology of Fishes*, 1991, **1**, 1–23.